Proceedings World Geothermal Congress 2020+1
Reykjavik, Iceland, April - October 2021

Development of a Geostatistical Thermal Model in the Great Basin Region, Western USA: A Pilot Study in Western Nevada

Whitney Trainor-Guitton[1], Cary R. Lindsey[2], D. Lane Boyd[1], Elijah Mlawsky[2], and Bridget Ayling[2]

[1]Department of Geophysics, Colorado School of Mines, Golden, CO 80401

[2]Great Basin Center for Geothermal Energy, University of Nevada Reno, Reno, NV 89557

caryl@unr.edu

Keywords: temperature, 3D, statistics, Great Basin, thermal model

ABSTRACT

The Great Basin region is a world-class geothermal province, spanning approximately 500,000 km² and including much of the states of Nevada and Utah, and parts of Idaho, Oregon and California. Currently, the Great Basin has ~ 1,100 MWe installed geothermal power generation capacity, and is estimated to have as much as ~10,000 MWe currently undiscovered potential (mean estimate). A major exploration challenge in the Great Basin is locating blind geothermal systems: as much as 2/3 of currently discovered systems are thought to be blind (i.e. have no surface thermal expressions). As such, understanding the subsurface temperature regime is imperative to guide more efficient geothermal exploration efforts in the basin, and improve exploration success. To date, substantial work and research has gone into studying temperatures in the basin by drilling temperature gradient wells, taking two-meter temperature probe measurements, and creating temperature maps at varying depths across the basin. However, to date, regional map products have been 2D in nature, and there has been no production of a true 3D temperature study of the Great Basin. Here, we present a 3D statistical model of the sub-surface temperatures in the area used for a previous Play Fairway Analysis in the Great Basin, by applying innovative geostatistical methods (such as sequential Gaussian simulation (SGSIM) for interpolation of the temperature field) to existing, publicly available temperature datasets. We also attempt to capture the effect of geologic structures on temperatures, given the known strong structural control on geothermal system occurrence in the Great Basin.

1. INTRODUCTION

As described in Witter et al. (2019), most geostatistical interpolation studies in geothermal have been in 2D. Many researchers have modeled temperatures in 2D using bottom-hole temperatures (BHTs) (Blackwell and Richards, 2004); shallow subsurface temperatures (Fairley et al., 2003; Lubenow et al., 2016; and Price et al., 2017); 2-meter temperature and geoprobe data (Zehner et al., 2012; Coolbaugh et al., 2014); and heat flow and other derivatives of temperature measurements (Williams and DeAngelo, 2011).

2D modeling of temperatures ignores the different variability in horizontal data versus vertical data, which this study proves is a strong characteristic of the 3D data. The 3D statistical approach has not been thoroughly explored in geothermal research but with the growth of geostatistics, multivariate statistics, and machine learning in geothermal exploration, tools are readily available to tackle the problem provided the data are available.

The data used for our model are part a larger data set compiled by Southern Methodist University (SMU, 2019). The entire dataset is available on the Southern Methodist node of the National Geothermal Data System. We relied solely on the SMU data for this pilot study; however, the Great Basin Center for Geothermal Energy continues to acquire and store geothermal datasets for the entire Great Basin. As these data are compiled, it will be possible to include more BHTs, 2-meter temperature data, geoprobe data, and any other relevant temperature data to refine the current model and expand the study across the Great Basin.

Refined temperature and heat flow maps lead to improved geothermal exploration and well targeting as well as advanced reservoir characterization pre-, during, and post-production. Here, we provide a 3D interpolation of BHTs in the pilot area in western Nevada.

2. STUDY AREA

The Great Basin, including virtually all of Nevada and areas in adjacent states, is part of the Basin and Range Province in the westem United States, an extensional province comprised of horsts and grabens. The extension in the Basin and Range has been active since the Miocene (Faulds et al., 2017). This extension and the subsequent creation of northeast-oriented range front and other complex Quaternary fault systems as well as the high geothermal gradient resulting from crustal thinning due to extension in the Great Basin creates a unique geothermal setting that currently hosts over 20 geothermal power plants (Figure 1b).

The study area in western Nevada (Figure 1a) has over 15 geothermal plants including Dixie Valley, Desert Peak, and Steamboat as well as several high profile geothermal prospects such as Fallon (Ayling et al., 2018), Gabbs Valley (Craig et al., 2017), and Granite Springs Valley (Faulds et al., 2019). The study is approximately the western half of the Nevada Play Fairway project, recent project funded by the Department of Energy. The Nevada Play Fairway is in the final stages of completion and the project achieved success in Gabbs Valley with the drilling of a temperature gradient well discovering approximately 120 °C fluid at 150 meters depth (Craig, 2019). In part because of the success of the Nevada project, we decided to focus our study on this area.

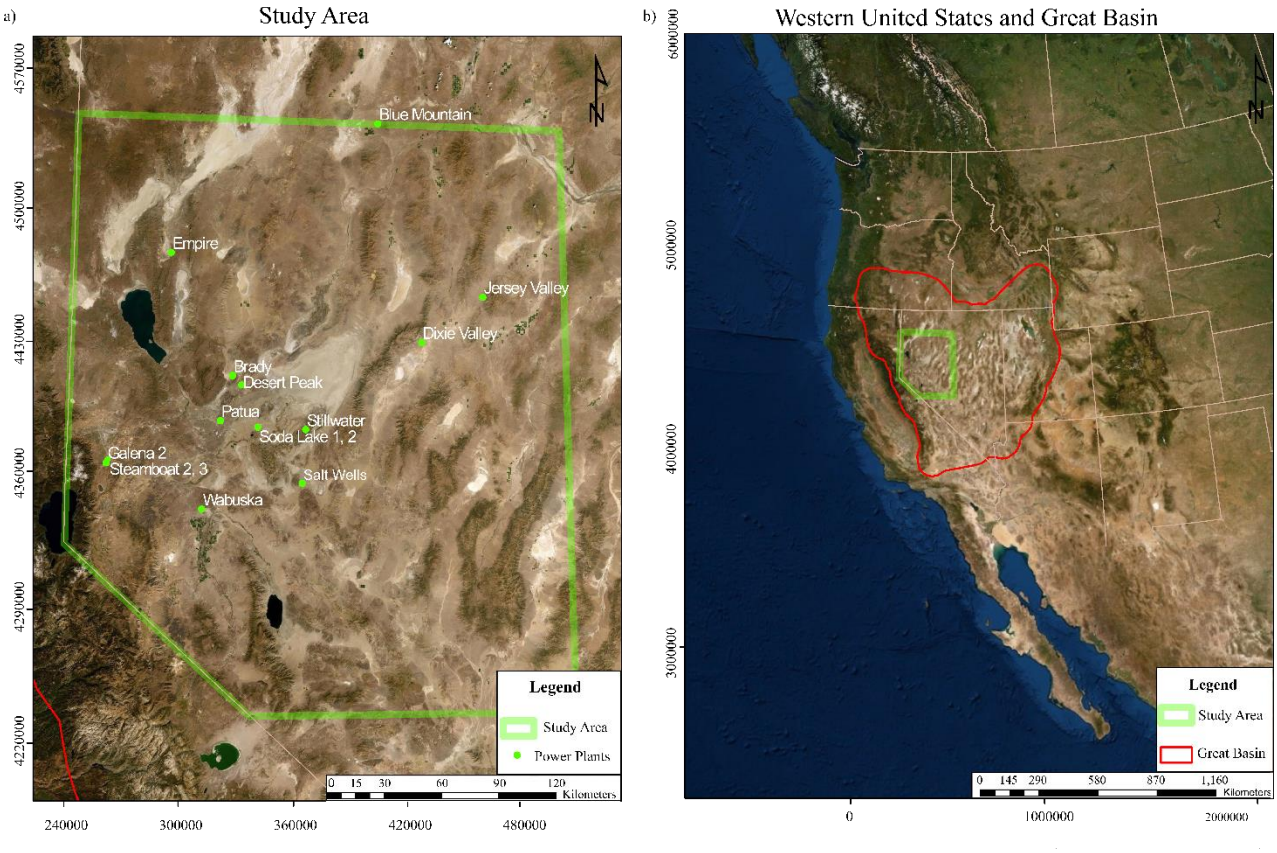

Figure 1: a) Study area with current power plants, b) western US with Great Basin and study area outlined.

3. DATA REVIEW

In order to retain lateral resolution, a subset of the regional filtered data (the whole Great Basin) was selected in western Nevada, with the dimensions of 240 km by 320 km. The 3D volume is represented by a 3D grid of 60x80x50 cells such that $dx=dy=4$ *km* and $dz=8$ *m*. The 3D volume (240 km by 320 km by 400 m) contains 1,555 BHT (bottom hole temperature) data points. An inside view of the 3D area is shown in Figure 2 from west looking east, south looking north, and in map view.

The highest recorded BHT was 283.7 °C from well NV-04853 in Dixie Valley. The measurement was also one of the deepest, taken at 3,551 m. The lowest recorded BHT was a well in Nye County with a BHT of 5.5 °C, drilled to approximately 40 meters. The mean value is 46.535 °C. The histogram of the data (Figure 3) shows a very distinct right skewedness as is common with geological phenomena. The majority of the data fall in the lower range value with fewer points exhibiting high values, which are often the sought-after values for geothermal explorers.

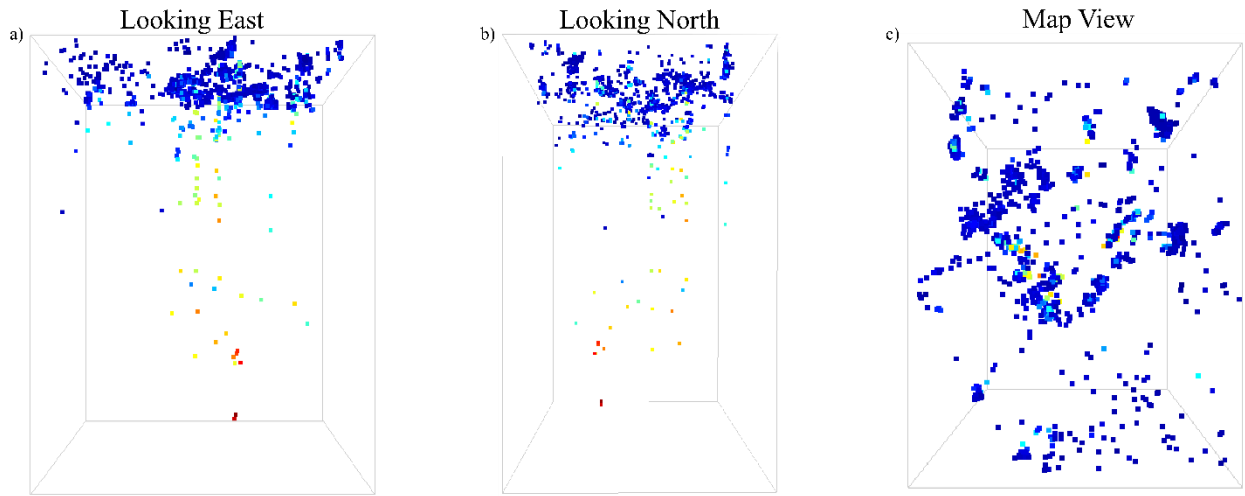

Figure 2: Subset of data used for 3D modeling: a) view looking north b) view looking east and c) and map view.

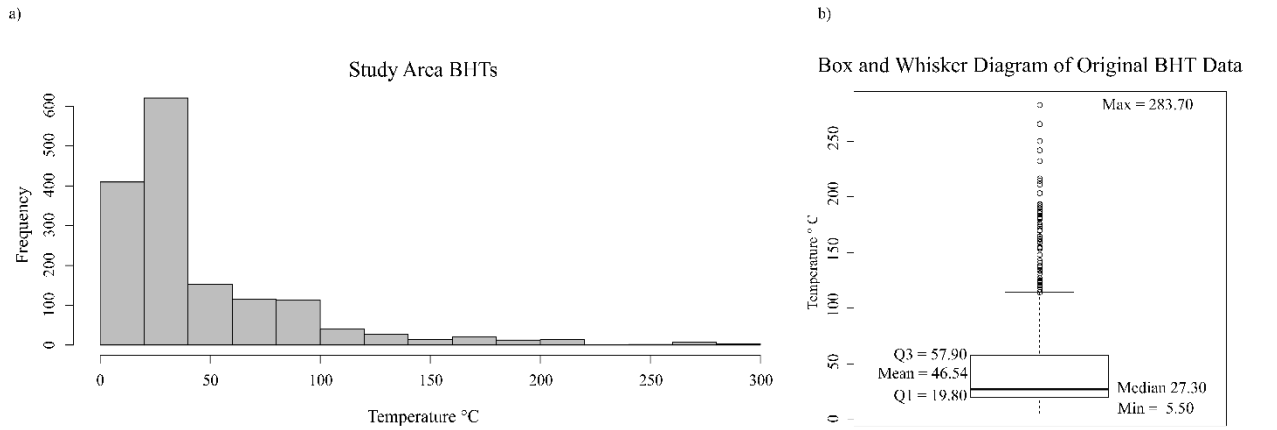

Figure 3: Distribution (a) and summary statistics (b) of BHT data used as 'hard data' in 3D modeling.

4. METHODS

We present both the 3D variogram modeling and 3D property modeling that produces many equiprobable models that are designed to reproduce the distribution and spatial correlation and also allow for P10 and P90 (10^{th} and 90^{th} percentile) temperature model calculations. These are created using Stanford's Geostatistical Modeling Software (SGEMS) (Remy et al., 2011).

4.1 3D Variogram Modeling

A 3D variogram captures the spatial correlation by a 3D ellipsoid: it is described by three radii (major, medium, minor) and three angles (dip, strike and rake) (Remy et al., 2011). The radii are known as ranges: they denote the distance in each respective direction at which data no longer have any correlation. These are represented along the x-axis of a 1D variogram, which is a slice of the 3D variogram ellipse. The y-axis of a 1D variogram denotes the actual variogram value γ

$$\gamma(h,\alpha,\beta,\theta) = \frac{1}{2N(h)}\sum_{i=1}^{N(h)}[z(u_i) - z(u_i+h)]^2 = \frac{1}{2}E\{[[z(u_i) - z(u_i+h)]]\} \qquad \text{Equation 1}$$

which measures the expected value of all square difference between pairs of data that comply with the distance separation, defined by h: $z(u_i)$ and $z(u_i+h)$. Vector $\boldsymbol{z}$ can represent any multitude of properties, e.g. temperature, permeability, porosity, etc., at location u_i. h is the distance vector separating the two data points. Note that this distance is in a particular angle direction; for 3D variogram modeling there are three angles: azimuth, dip and plunge/rake or $\alpha, \beta,$ and θ. Given non-exhaustive, spatial dataset, it is both challenging and imperative to define tolerances on both h and $\alpha, \beta,$ and θ, in order to define enough pairs of data $\boldsymbol{z}$ to have robust variogram (Remy et al., 2011).

For the study area, nine directions were calculated with the following azimuth and dip (rake was kept at 0): (0,0), (30,0), (60,0), (90,0), (0,90), (30,45), (45,45), (60,45), and (90,45). Three of these are shown in Figure 4 as black circles. In order to better visualize the 3D calculation, the vertical units were exaggerated by a factor 1000, to account for the greater lateral coverage as compared to the depth. The lag tolerance on h was set to +/-10km and angle tolerance on θ was set to +/-10°.

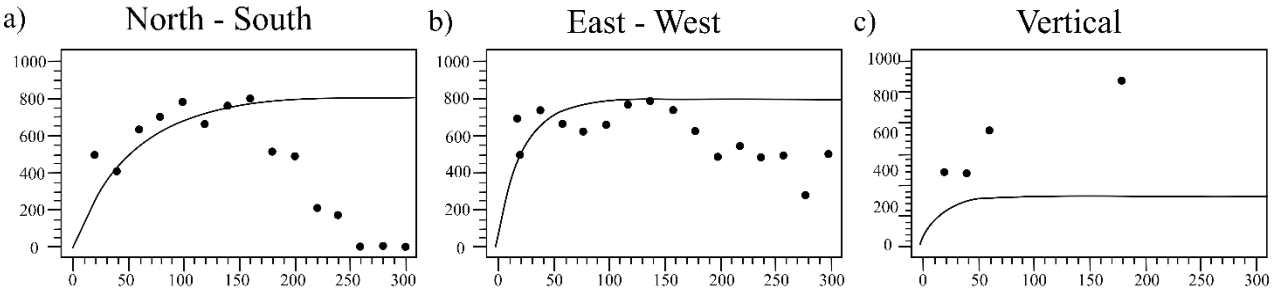

Figure 4: Observed (circles) and modeled variogram (line) for 4 directions a) major range of 165 km in North-South b) medium range of 65km East-West c) minor range 56m in vertical. The y-axis depicts the variance and note the higher variance in the Vertical (~3000) versus laterally (800).

From these 1D slices, the SGEMS software allows for the users to define the angle of maximum continuity and the distances of the radii to fit a variogram model to the data. A model variogram (black line in Figure 4) was fit to the observed (or experimental) variogram, shown as black circles. The model variogram is laterally anisotropic and exponential, with the major range direction of north with magnitude ~150 km (a). Given the orientation of the Basin and Range, this is reasonable. The medium and minor radii and directions are ~65 km East-West (Figure 4b) and 56 m vertically (Figure 4c). Note the factor three difference in the sill (y-axis values): these variograms have zonal anisotropy (Isaaks and Srivastava, 1989; Deutsch, 2002). The effect on the kriging system of equations is that the vertical component of variability will not contribute to horizontal (Deutsch and Journel, 1998). The variogram

modeling within SGEMS does not explicitly allow for fitting different sill values in different directions. The effect of this on the final realizations and future remedies is reviewed in the Discussion (section 6).

4.2 Stochastic Geostatistics

Sequential Gaussian Simulation (SGSIM) is a well-known and utilized algorithm that stochastically simulates petrophysical properties using (and reproducing) a given variogram and histogram (Deutsch and Journel, 1998). SGSIM defines a Gaussian probability density function where the mean (μ) and variance (σ) are set to the Kriging estimate and variance, respectively, in the normal-score space. The algorithm then uses a Monte Carlo draw to determine the estimation of a property ($\boldsymbol{z}$) at a particular location ($\boldsymbol{u}_0$) within the grid.

$$z(\boldsymbol{u}_0) = N(\mu, \sigma) \quad \forall\, \boldsymbol{u} \qquad \text{Equation 2}$$

The algorithm reproduces the variogram by using previously simulated values for future estimates, unlike Kriging that will only use the original hard data (e.g. the 1,555 BHT data points) that are within the range.

The 3D grid defined in the introduction (60x80x50) are used to build the SGSIM realizations. Figure 5 contains four example realizations, all shown with the same color threshold: minimum = 5°C and maximum = 285°C.

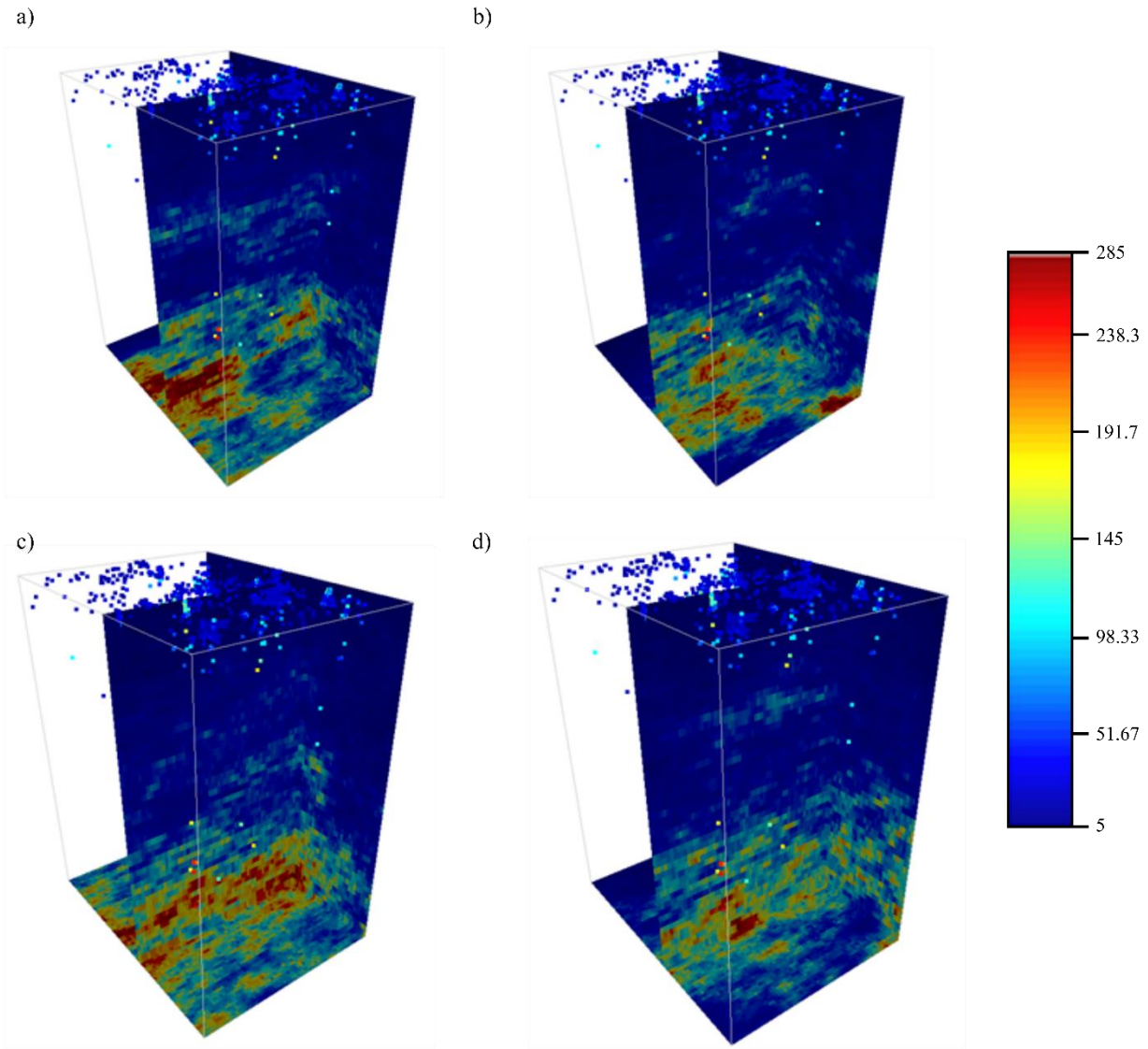

Figure 5: Four example realizations shown with hard data and highlighting slice y=47 a) Realization 0, b) Realization 12, c) Realization 27, and d) Realization 33. Temperatures in °C.

5. RESULTS

The advantage of having many models (50 realizations in our study) is the ability to assess the variability, the quantiles (percentiles) and probability to be above certain temperature thresholds within the 3D volume of interest. These types of quantitative interpretations cannot be done with one kriging solution.

5.1 Probability of Exceeding Threshold

First, we calculate at each cell within the 3D model, the probability of that location exceeding defined temperature thresholds. This type of interpretation is important for making well-placement decisions. Figure 6 contains the probability of exceeding a) 100°C, b) 150°C, and c) 200°C, shown at the same y = 47 slice.

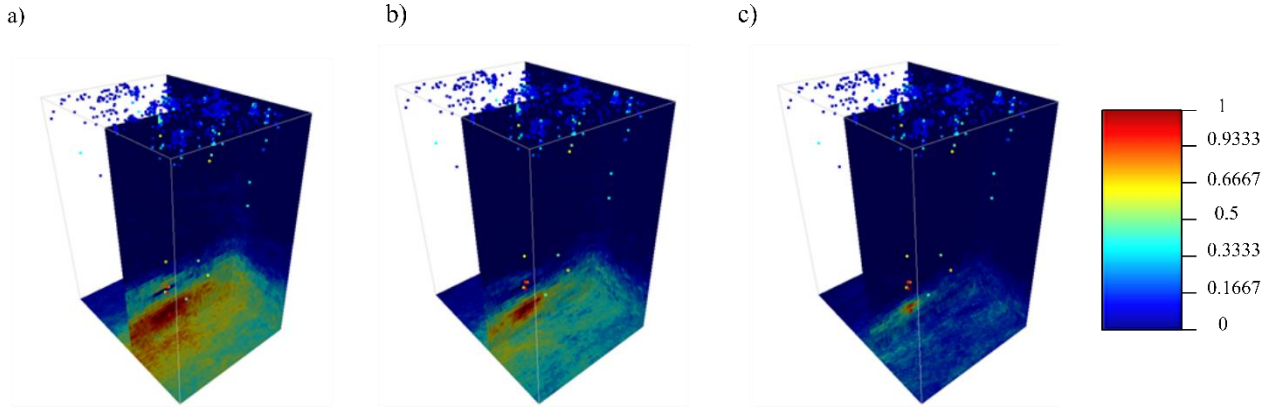

Figure 6: Probability of exceeding defined temperature thresholds a) 100 °C b) 150 °C c) 200 °C

5.2 Reproducing Statistics

As described previously, one advantage of using stochastic simulation is that the histogram and variogram are reproduced, unlike with a kriging result. Comparing Figure 3 and Figure 7, we see that the shape and more precisely the maximum, minimum, and quartiles are comparable. However, the variance is slightly higher for the SGSIM example realization (2,009) than the original BHT dataset (1,990).

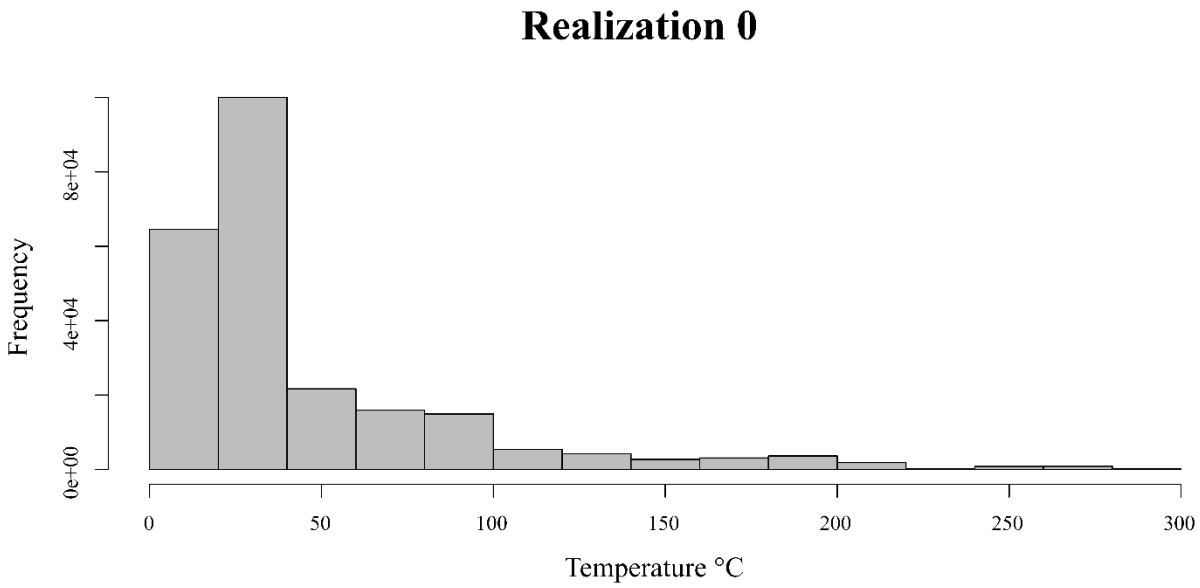

Figure 7: Histogram of Realization 0 that has an equivalent shape and summary statistics to Figure 3.

Now we compare the input (variogram model in black in Figure 4 to the output variogram of the Realization 0 in Figure 5a. The same variogram model (black) from Figure 4 is shown in Figure 8, but now the distance units are in terms of the cell dimensions for any particular direction. Recall, the major range (radius) was in the direction of North-South for 152 km. Since dy=4 km, this would be 152 km / 4 km = 38 cell units (Figure 8a). Similarly, the medium range is East-West, 64 km / 4 km = 16 units (Figure 8b), and the minor range is vertical with dz = 8 m, such that 56 m / 8 m = 7 (Figure 8c). The data count is now 24,000 with a mean of 45.4497, a highest value of 283.993 and a minimum value of 5.09623, which is consistent with the raw data (Figure 3).

The red variograms are calculated from Realization 0 (Figure 5a). We see a good match between the input (black) and output (red) variogram for the North-South direction. However, there is less of an ideal fit for the other two directions. Note the higher sill value in the East-West plot (Figure 8b). The vertical variogram behavior is an example of non-stationary variogram: the variance continues to increase, never leveling off to a sill value. This is likely due the zonal anisotropy observed in the raw data (or experimental variogram of Figure 4).

5.3 E-type and P50 models

The average or e-type (short for expectation) can be calculated from the 50 SGSIM realizations. If more realizations were computed, the e-type would approach the kriging estimate. Due to data sparsity at lower depths, computing the kriging model resulted in many undefined values in the deeper model space. Thus, the e-type can be a substitute for the kriging model, which is designed to provide an unbiased, conservative estimate.

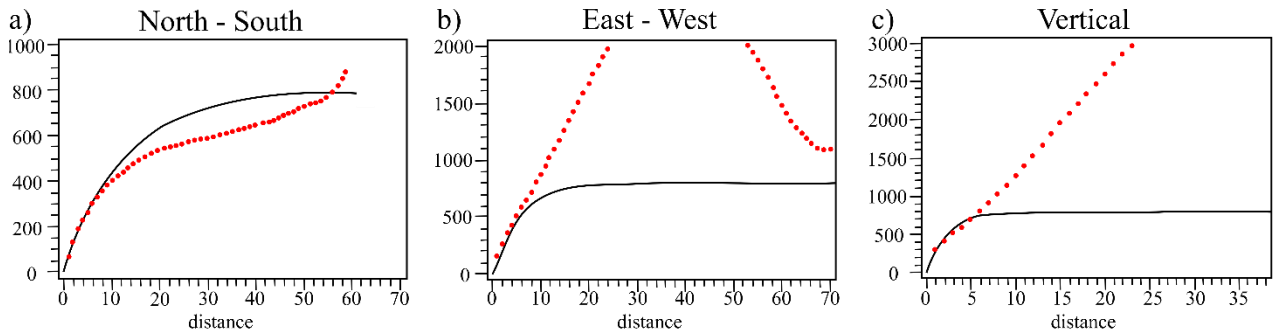

Figure 8: Calculated variogram from Realization 0 (red) compared to modeled variogram of BHT data (black) a) North-South in units of dy (4 km), b) East-West in units of dx (4 km), c) vertical in units of dz (8 m)

We compare the E-type to the P50 (50th percentile) model or the median value for each location across all 50 realizations. The minimum, maximum and lower quartile for both are roughly equivalent; the mean, variance, upper quartile and median are all higher for the e-type versus the P50 model. This reveals how the expectation (arithmetic average) is more influenced by the high temperature values present in some realizations, originating from the right skew of the original BHT data (Figure 3). We want to keep the skew and make many sequential Gaussian simulations of that skew because that is where the economic temperatures are represented.

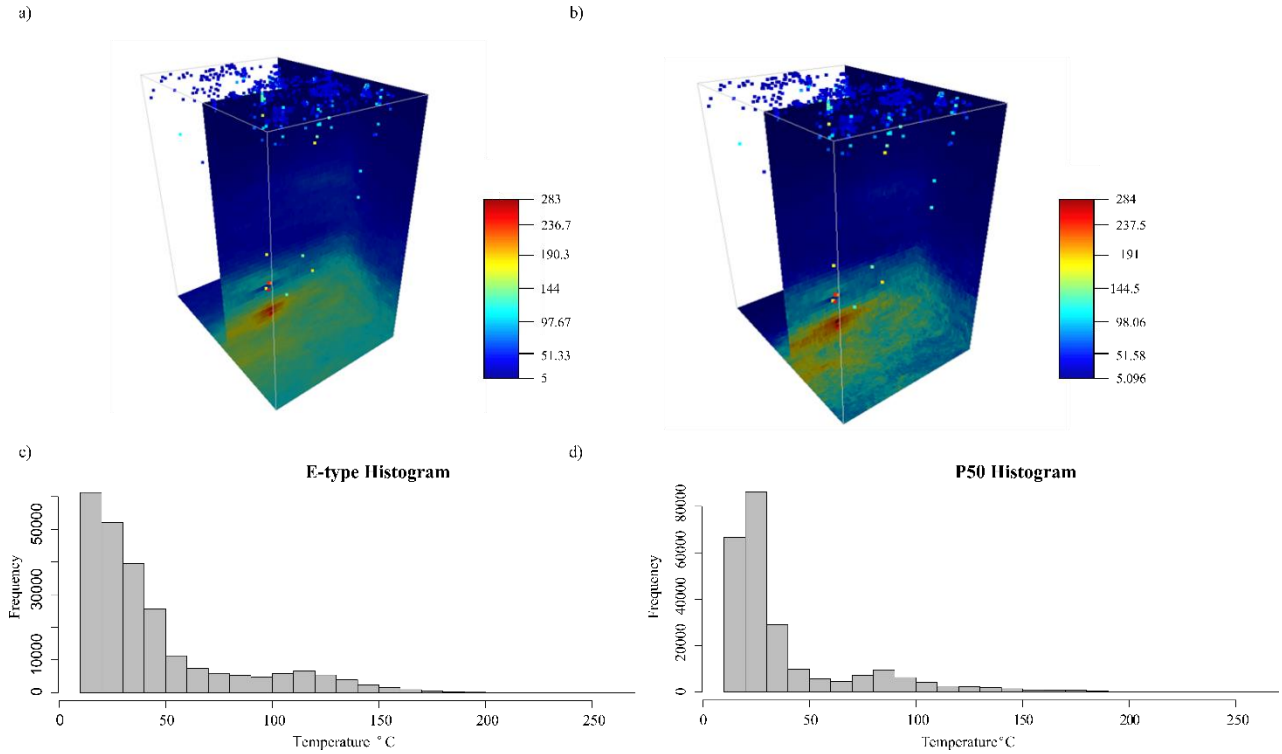

Figure 9: a) E-type and b) P50 model with their respective distributions

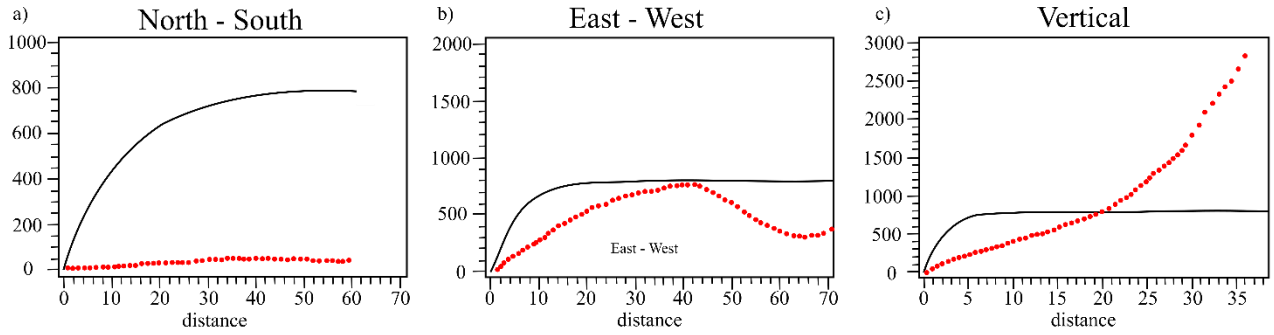

Figure 10: Calculated variograms of E-type (red) compared to modeled variogram of BHT data (black) a) North-South, b) East-West, c) vertical.

Figure 10 again compares the input (variogram model in black in Figure 4 and Figure 8) but now to the output variogram of the E-type model in Figure 9. Although the SGSIM variograms did not perfectly recreate the experimental variograms, they have performed much better than the mismatch shown in Figure 10. Here, the ranges of the E-type (red) are all much greater than the data equivalent (black), giving a very smooth estimate model. This is expected from an average, which is representative of a kriging model.

6. DISCUSSION

Reproduction of the input variogram was better in the SGSIM realizations than in the E-type or P50 model. However, the output variograms from the realization were deficient. We believe two approaches may improve this. First, transforming the distribution of the data initially may allow for more stable variogram modeling and better reproduction (Kelkar and Perez, 2002). This would require two extra steps: an initial transform and back-transform after the SGSIM generation.

After further inquiry, it was found that differing sills are often modeled with a nested variogram structure, where an infinite range in the direction of with a lower sill (Deutsch and Journel, 1998); therefore, it could be incorporated into the SGEM's variogram modeling. For example, the fitted model only used one exponential model with major range direction North and magnitude ~150 km. This variogram model accounted for 100% of the sill. To better account for the different sill in the vertical direction, a second model could be added that has a very large range in the horizontal direction and would account for some percentage of the sill. The very large range would cancel the contribution of that structure along that direction (for our case horizontal).

7. CONCLUSIONS

This work provides the first stochastic analysis of 3D temperature data, providing P10, P50 and P90 models of temperature, and probability of exceeding certain temperature thresholds, which are more useful decision-making tools for geothermal explorers. Given the 3D nature of geology, it is imperative to include the 3D spatial correlation when making models and decisions for future drilling locations.

Further work will improve the inclusion of zonal anisotropy but also explore other styles of kriging such as co-kriging to include other types of data that are available in the area. Geochemistry, stratigraphy, and proxies for permeability are available for the area. All three types of data could be included in co-kriging models that can utilize the spatial correlation between the two different properties. Boyd et al. (2018) provide a novel way to include stratigraphy data as the secondary data in co-Kriging, which is typically more spatially-exhaustive than the primary data, such as these sparse temperature data.

REFERENCES

Ayling, B., and Blankenship, D.: Phase 2 update for the Fallon FORGE site, Nevada, USA. *Proceedings*, 43rd Workshop on Geothermal Reservoir Engineering, Stanford University, (2018). SGP-TR-213.

Blackwell, D.D., and M.C. Richards, 2004, Geothermal Map of North America, American Association of Petroleum Geologists.

Boyd, D.L., Walton, G., and Trainor-Guitton, W., 2018, Improving geological models through statistical integration of borehole data and geologists' cross-sections, *in* 52nd U.S. Rock Mechanics/Geomechanics Symposium,.

Deutsch, C. V., 2002, Geostatistical Reservoir Modeling: New York, Osford University Press, 124–152 p.

Deutsch, C. V., and Journel, A.G., 1998, GSLIB: Geostatistical Software Library and User's Guide.: New York, Oxford University Press.

Isaaks, E., and Srivastava, R., 1989, An introduction to applied geostatistics: Oxford Univ. Press, New York, 561 p.

Kelkar, M., and Perez, G., 2002, Applied Geostatistics for Reservoir Characterization: Society of Petroleum Engineers, 264 p.

Remy, N., Boucher, A., and Wu, J., 2011, Applied Geostatistics with SGeMS: A User's Guide: Cambridge University Press, 264 p.

Witter, J.B., Trainor-Guitton, W.J., and Siler, D.L., 2019, Uncertainty and risk evaluation during the exploration stage of geothermal development: A review: Geothermics, v. 78, p. 233–242, doi: 10.1016/j.geothermics.2018.12.011.